Journal of Electrical Engineering & Technology (2025) 20:3875–3887
https://doi.org/10.1007/s42835-025-02334-y

ORIGINAL ARTICLE

Simulation-Based Evaluation of Power Efficiency and Output Capacitance in Standalone PV MPPT Buck Converters Using 200 V *p*-GaN HEMTs

Xinzhi Liu[1,2] · Suhaidi Shafie[1,3,4] · Mohd Amran Mohd Radzi[1,2] · Norhafiz Azis[1,2] · Abdul Hafiz Abdul Karim[1,2,5] · Nurbahirah Norddin[1] · Ismail Lawal[1,3]

Received: 22 March 2024 / Revised: 19 April 2025 / Accepted: 12 May 2025 / Published online: 30 June 2025

Abstract

This study addresses the inefficiencies and limitations of conventional silicon-based MOSFETs in photovoltaic (PV) Maximum Power Point Tracking (MPPT) buck converters by introducing a simulation based approach to assess 200 V Schottky *p*-GaN High Electron Mobility Transistors (HEMTs). Motivated by the need for more efficient and reliable renewable energy solutions, the study explores the advantages of Gallium Nitride (GaN) devices in overcoming challenges such as limited power capacity, poor efficiency, and heat dissipation inherent in traditional semiconductors. By integrating MATLAB Simulink and SPICE simulation techniques, the transfer characteristics of GaN HEMTs are compared against those of MOSFET and Silicon Carbide (SiC) devices, with a specific focus on the impact of output capacitance (C_{OSS}) extraction on system performance. A duty cycle controlled Perturb and Observe (P&O) MPPT algorithm is introduced, and a comprehensive evaluation of a standalone PV array under varying irradiance conditions is conducted. The analysis extends to a hard-switching multi-pulse test under constant input, contrasting GaN with MOSFET and SiC devices to highlight GaN's superior efficiency and suitability for remote energy applications. Conclusive simulations reveal that 200 V *p*-GaN HEMTs exhibit 2.24 times lower average power losses during hard-switching cycles compared to MOSFETs, demonstrating their exceptional performance in optimizing standalone PV MPPT buck converters. This advancement significantly contributes to enhancing the efficiency and reliability of renewable energy systems globally.

Keywords *p*-GaN HEMTs · Standalone PV MPPT buck converters · MPPT · Output capacitance · Energy efficiency

✉ Suhaidi Shafie
suhaidi@upm.edu.my

Xinzhi Liu
berryxinzhiliu@hotmail.com

Mohd Amran Mohd Radzi
amranmr@upm.edu.my

Norhafiz Azis
norhafiz@upm.edu.my

Abdul Hafiz Abdul Karim
akahafiz@unimas.my

Nurbahirah Norddin
nurbahirah@utem.edu.my

Ismail Lawal
ismo4faty2015@gmail.com

1 Department of Electrical and Electronic Engineering, Universiti Putra Malaysia, Selangor 43400, Malaysia

2 Advanced Lightning, Power, and Energy Research (ALPER) Centre, Universiti Putra Malaysia, Selangor 43400, Malaysia

3 Institute of Nanoscience and Nanotechnology, Universiti Putra Malaysia, Serdang, Selangor 43400, Malaysia

4 Institute of Nano Electronic Engineering, Universiti Malaysia Perlis, Kangar 01007, Malaysia

5 Department of Electrical & Electronics Engineering, Faculty of Engineering, University Malaysia Sarawak (UNIMAS), Kota Samarahan, Sarawak 94300, Malaysia

Abbreviations

PV	Photovoltaic
MPPT	Maximum Power Point Tracking
GaN	Gallium Nitride
HEMTs	High Electron Mobility Transistors
SiC	Silicon Carbide
C_{OSS}	Output capacitance
2DEG	Two-dimensional electron gas
GIT	Gate Injection Transistors
EVs	Electric vehicles
V_{DS}	Drain-source voltages
LGA	Land Grid Array
$R_{DS(ON)}$	Dynamic on-resistance
I_{PV}	Produced photovoltaic current
V_{PV}	Produced photovoltaic voltage
DC	Direct current
D	Duty cycle
PWM	Pulse-width modulation
R_{load}	Load resistor
L_{buck}	Buck inductor
C_{buck}	Buck capacitor
P&O	Perturbation and Observation
D_{init}	Starting duty cycle
dV	Change in voltage
C_{ISS}	Input capacitance
C_{RSS}	Reverse transfer capacitance
C_{GD}	Gate-to-drain capacitance
DUT	Device under test
V_{GS}	Gate-to-source voltage

1 Introduction

Energy issues and environmental degradation are exacerbated by our dependence on fossil fuels, which is further exacerbated by the rapid growth of industrial activity and the global population [1–6]. This matter emphasizes the importance of solutions that are derived from renewable energy sources [4, 7, 8]. Solar photovoltaic energy is a prominent alternative that offers a pure and inexhaustible power source [3, 6, 9, 10]. Off-grid solar photovoltaic systems offer numerous benefits in remote regions where it is impractical to connect to the primary power infrastructure [11–14]. These configurations enable the direct energizing of devices or the charging of storage batteries using solar electricity. This is made possible by DC-DC converters that modulate the voltage to optimize device performance [15–18].

The rising use of solar photovoltaic systems necessitates improvements in the efficiency and endurance of energy conversion technology. Conventional silicon-based Metal-Oxide-Semiconductor Field-Effect Transistors (MOSFETs) are widely used in power conversion applications, but they have inherent limitations such as high on-resistance, and significant switching losses due to slower switching speeds [19]. These problems contribute to insufficient heat dissipation and limited power handling capabilities, rendering silicon MOSFETs unsuitable for high-efficiency, high-power applications. Silicon Carbide (SiC) devices, as wide-bandgap semiconductors, have evolved to address some of these constraints by providing greater breakdown voltages and better thermal conductivity than silicon devices [20]. However, SiC devices continue to encounter issues such as reduced switching frequencies owing to increasing gate charge and capacitance, and manufacturing process complications. These constraints restrict their effectiveness in applications needing very fast switching rates and efficiency.

In contrast, Gallium Nitride (GaN) High Electron Mobility Transistors (HEMTs) are gaining popularity in power electronics owing to their better material features, including greater electron mobility, a bigger critical electric field, and a broader bandgap energy [21, 22]. These features allow GaN HEMTs to switch quicker, have lower on-resistance, and be more efficient at high frequencies than silicon MOSFETs and SiC devices. GaN HEMTs' distinctive AlGaN/GaN heterostructure promotes the development of a two-dimensional electron gas (2DEG), which adds to their superior electrical performance [23].

Two recent advances in GaN device technology are Schottky p-GaN HEMTs and Gate Injection Transistors (GITs). In Schottky p-GaN HEMTs, the gate creates a metal-semiconductor (Schottky) junction above a *p*-type GaN layer, allowing normally-off operation and enhanced gate control, both of which are critical for energy efficiency and safety in power applications. In contrast, GIT devices modify conductivity by introducing holes into the channel via a *p*-type gate mechanism, enabling a fail-safe operating mode that is particularly favorable for some applications [24].

Schottky *p*-GaN HEMTs are ideal for applications that need fast switching, high frequency, and high efficiency, such as RF amplification, AC-DC power supply, and DC-DC converters. GITs, on the other hand, are better suited to applications requiring great power density and dependability, such as high-voltage DC transmission systems and electric vehicles (EVs). Standard GaN HEMTs made using lateral AlGaN/GaN methods may support drain-source voltages (V_{DS}) of up to 650 V. Many manufacturers provide devices in small packaging with voltage ratings ranging from 30 V to 300 V to meet a broad variety of power applications. Figure 1 depicts the commercial Schottky *p*-GaN HEMT structure, which demonstrates the complicated engineering and design techniques used in these high-performance devices [25, 26].

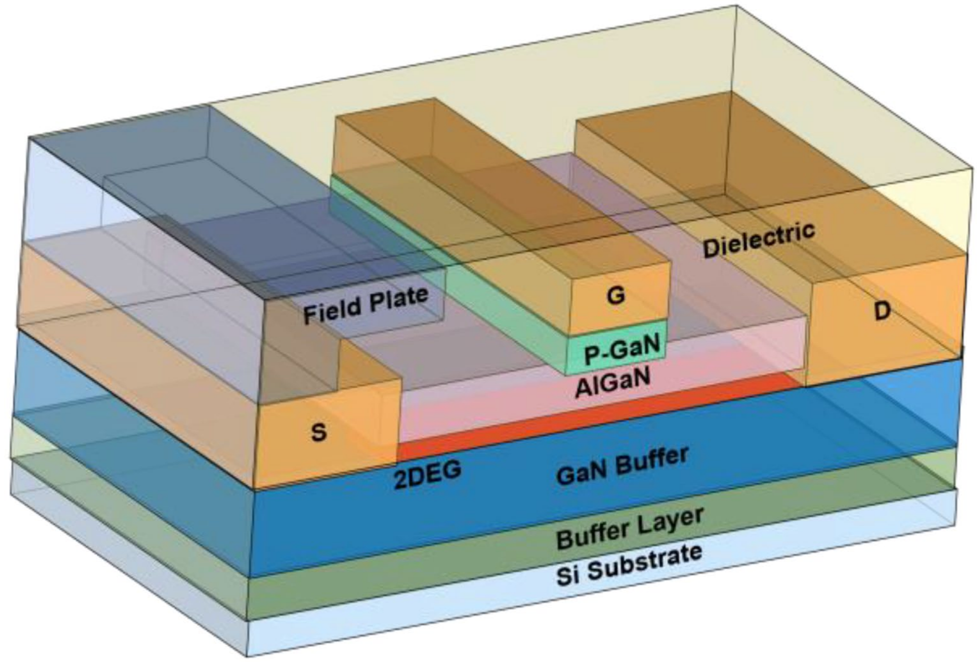

Fig. 1 Typical structure of Schottky *p*-GaN HEMT

GaN devices have developed numerous defects, despite their remarkable semiconducting properties, notably in power applications for solar PV converters. The hot electrons generated at the AlGaN/GaN heterojunction are the cause of the aberrant gate voltage threshold and potential device instability, which subsequently migrate into or become confined within the buffer or dielectric layers. Additionally, GaN HEMTs demonstrate a significantly lower gate breakdown voltage than conventional Metal-Oxide-Semiconductor Field-Effect Transistors (MOSFETs). In high-frequency power converter applications, this may result in irreversible device failure due to the generation of spikes or surges at the gate in conditions of elevated dv/dt or parasitic inductance. Charge trapping events are also responsible for fluctuations in dynamic on-resistance ($R_{DS(ON)}$), which lead to increased conduction losses in power applications [24]. In order to reduce ringing disturbances caused by elevated dv/dt and di/dt rates, it is imperative to implement meticulous circuit design, despite the exceptional fast-switching capabilities of GaN devices. Companies like Efficient Power Conversion (EPC) have implemented Land Grid Array (LGA) packaging for applications that require reduced power consumption. This method reduces dimensions while increasing output capacitance as a result of the increased number of drain and source connections. In half-bridge topologies, the simultaneous operation of switches can result in the elevation of switching losses due to the interaction among capacitances [25].

Recent advances in GaN HEMT converters, notably for solar PV applications, have resulted in better circuit designs and modeling capabilities, particularly in non-isolated converter arrangements. Suskis et al. (2014) developed a synchronous boost MPPT converter employing GaN switches, attaining a theoretical efficiency of 98.9% using the SPICE EPC2001 model [27]. However, this research employed a constant voltage source for the PV input and did not include PV maximum power point tracking (MPPT) modeling, input scenario analysis, or a comparison of GaN HEMTs with silicon MOSFETs and SiC technology. Similarly, Alharbi (2017) created a non-isolated DC-DC buck-boost converter using a TPH3206PD cascade GaN-FET and a CPW2-0600-S010B SiC-Schottky diode, which achieved a simulated efficiency of 95.3% at 100 kHz [28]. This research did not properly investigate variable frequencies, power losses, or specific converter efficiency measures.

Empirical assessments show that GaN DC-DC converters are very efficient in real applications. Mikołaj (2021) tested four buck-boost converters using Si MOSFETs and E-GaN HEMTs in SEPIC and cascaded topologies, obtaining a maximum efficiency of 96.5% at 180 kHz [29]. However, this study did not look into PV applications or MPPT integration. Mdanat (2020) examined switching waveforms for GaN, MOSFET, and SiC devices in a 15-kW converter [30]. The lack of parasitic inductance in the models made them idealized and less convincing for real applications. Furthermore, the high-power output surpassed GaN's optimum range, restricting its suitability for medium-voltage applications. Alharbi (2021) investigated medium-voltage bidirectional DC-DC converters by comparing Si-MOSFET, SiC MOSFET, and cascade GaN HEMT technologies [31]. The GaN HEMT design achieved 96.2% efficiency with a 96 V input at 40 kHz. Nonetheless, this research did not include PV MPPT applications, emphasizing the need of application-specific studies to fully comprehend the potential of GaN HEMT converters in solar energy systems.

These investigations point to substantial limitations in the applicability of GaN HEMT technology to PV MPPT systems. Much of the current research focuses on enhancing MPPT approaches in simulation settings using idealized MOSFET models, frequently missing the nuances of semiconductor device performance under different operating situations. Investigations on the electrical properties of GaN HEMTs and SiC devices often focus on circuit features rather than completely examining their integration with PV MPPT systems.

This study addresses these deficiencies by presenting a simulation-based method that integrates PV MPPT algorithm creation with GaN HEMT circuit analysis. This work uses MATLAB Simulink and SPICE simulation techniques to analyze the transfer characteristics of GaN HEMTs in comparison to traditional MOSFET and SiC devices, focusing specifically on the impact of output capacitance (C_{OSS}) extraction on system efficiency. This comprehensive research encompasses the implementation of a duty cycle-controlled P&O MPPT algorithm in a standalone 4-series PV array under diverse irradiance conditions, along with an in-depth analysis of hard switching performance. This study emphasizes the superior efficiency and potential of GaN HEMTs in enhancing standalone PV MPPT buck converters using an integrated research methodology, marking a significant advancement in the global pursuit of reliable and efficient renewable energy sources.

The document is structured as follows: Sect. 2 delineates the proposed photovoltaic maximum power point tracking buck converter system, including a duty-cycle-based perturb and observe maximum power point tracking control and a method for assessing parasitic capacitances in gallium nitride high electron mobility transistors. Section 3 delineates the modeling and performance assessment of the proposed system using MATLAB Simulink, including photovoltaic input and output characteristics under diverse solar irradiation conditions. Section 4 advances the discourse with a SPICE Simulation Analysis of GaN HEMTs tailored to the requirements of the PV converter, highlighting static transfer and output capacitance characteristics while examining power losses via hard-switching tests. The paper concludes by examining key results and their implications, underscoring the significant advancements made in enhancing PV MPPT systems via the use of GaN HEMTs.

2 Methodology

2.1 Proposed PV MPPT Buck Converter Scheme

Figure 2 illustrates a schematic of a self-sufficient PV system that incorporates an MPPT mechanism within a buck converter layout. This system features an array of four PV panels serially connected, each converting solar radiation into direct current (DC). The produced current (I_{PV}) and voltage (V_{PV}) from the array are directed to an MPPT controller. This controller adjusts the duty cycle (D) of a pulse-width modulation (PWM) signal to maximize power capture, responsive to the changing solar irradiance and ambient temperatures. The MPPT buck converter's functionality is driven by two *p*-GaN HEMTs, Q_1 and Q_2. These switches cycle between conduction and non-conduction states as dictated by the PWM signal, thus reducing the voltage from the PV array to levels conducive for battery storage or direct consumption by the load (R_{load}). The absence of a reverse recovery characteristic in *p*-GaN HEMTs obviates the need for an external Schottky diode, with Q_2's switching, managed by precise dead-time control, effectively preventing reverse currents. Integral to the converter's operation, the inductor

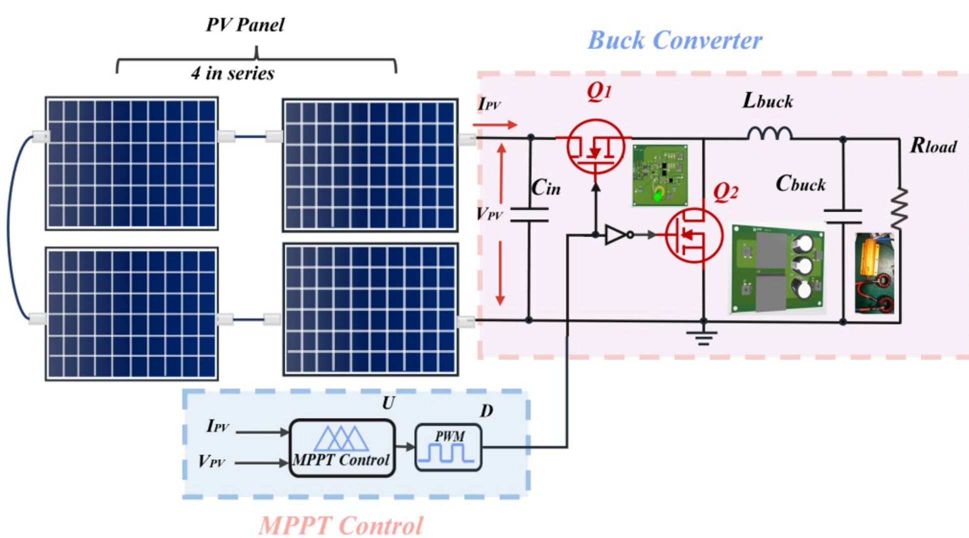

Fig. 2 Schematic of proposed standalone PV MPPT buck converter

(L_{buck}) and capacitors (C_{buck} and C_{in}) mitigate the pulsating nature of the switched output, ensuring a consistent DC supply. The inductor modulates current rate changes, accumulating energy when Q_1 is energized and dispensing it upon deactivation. The capacitors act to smooth out voltage fluctuations, further refining the output. The energy is thus made accessible for powering loads or recharging batteries. The MPPT controller, through a feedback system, oversees the power output, persistently fine-tuning the PWM duty cycle to secure operation at the MPP of the PV panels.

2.2 Duty-Cycle-Based Perturbation and Observation MPPT Control

As delineated in Fig. 3, the Duty-Cycle-Based Perturbation and Observation (P&O) algorithm was selected for Maximum Power Point Tracking (MPPT) due to its proven reliability, simplicity of implementation, and straightforward control structure, making it highly suitable for practical photovoltaic (PV) system deployments. Although advanced MPPT techniques, such as fuzzy logic or neural network-based algorithms, have been developed, they often introduce complexity in control design, require extensive training data, and demand increased computational resources. In contrast, the Duty-Cycle-Based P&O algorithm offers an effective balance of simplicity and robustness, making it ideal for scenarios demanding reliability and ease of implementation. This control scheme adeptly iterates the adjustment of the power converter's duty cycle to pinpoint the MPP amidst fluctuating solar irradiance levels. Initially, the algorithm is configured with predetermined limits for the maximum (D_{max}) and minimum (D_{min}) duty cycles, in conjunction with a starting duty cycle (D_{init}) and a nominal perturbation magnitude (ΔD). With each iteration, the algorithm calculates the product of the PV voltage (V_{PV}) and current (I_{PV}) to ascertain the current power output (P_{PV}), comparing it with the preceding iteration's power (P_{old}) to gauge the directional change in power. Simultaneously, it evaluates the change in voltage (dV) to determine the appropriate direction for duty cycle perturbation. In instances where power output decreases ($dP<0$), it inversely adjusts the duty cycle direction. Conversely, a positive dP, indicative of a power increase, prompts continuation in the same direction of perturbation. The adjustment of the duty cycle (D) is executed in fine increments ΔD, strictly within the designated D_{max} and D_{min} boundaries, to ensure the system's operation remains within optimal and safe parameters. The algorithm leverages persistent variables (V_{old}, P_{old}, D_{old}) to retain the voltage, power, and duty cycle values from the previous cycle, thus enabling an efficient comparative analysis for subsequent perturbations. Through this iterative process, the algorithm proficiently traces the MPP, thereby maximizing the PV system's power generation.

2.3 Measurement of Parasitic Capacitances in GaN HEMTs

The output capacitance (C_{OSS}) of GaN HEMTs, defined as the combination of drain-source capacitance (C_{DS}) and gate-to-drain capacitance (C_{GD}), plays a crucial role in half-bridge topologies, directly influencing switching performance through charge-discharge cycles across the device parasitic capacitances. Specifically, C_{OSS} significantly impacts converter design, particularly in soft-switching

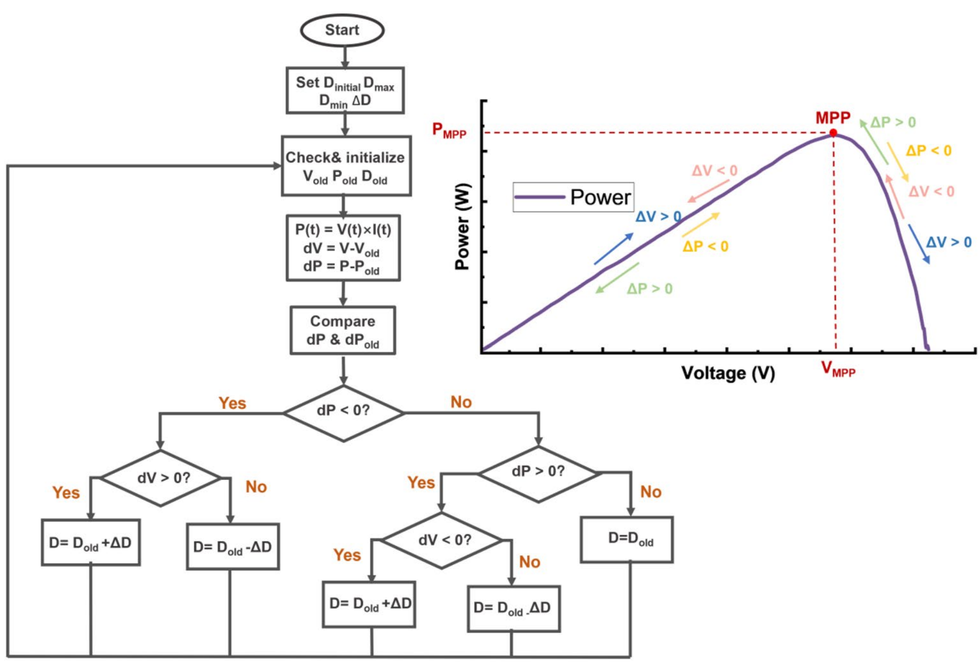

Fig. 3 Flowchart of duty-cycle-based perturbation and observation MPPT control

applications, where accurate characterization of the device's capacitive behavior is vital for achieving efficient zero-voltage switching transitions. Additionally, the input capacitance (C_{ISS})—measured with the drain and source terminals shorted—determines the total gate charge required for transitioning the transistor between conduction states. The reverse transfer capacitance (C_{RSS}), commonly referred to as Miller capacitance, critically influences switching performance through the Miller effect, where gate-to-drain coupling induces feedback, potentially causing voltage transitions to reflect amplified disturbances at the gate.

Moreover, the significance of C_{OSS} becomes more pronounced at higher switching frequencies, as frequency-dependent trapping effects and depletion region modulation alter the effective C_{DS}. Although the intrinsic value of C_{OSS} is not directly frequency-dependent, increased switching frequencies intensify trapping and de-trapping dynamics within the GaN HEMT's buffer and barrier layers, subsequently affecting the depletion layer width and thus dynamically modifying the device's C_{DS}. Hence, a thorough understanding of C_{OSS} behavior across various switching frequencies is essential for precise design and optimal performance prediction in GaN-based power converters [32].

Figure 4 illustrates the setup for extracting parasitic capacitances in GaN HEMTs, suitable for both measurement and simulation. To initiate this process, a high-frequency impedance analyzer is used to generate a small-signal sinusoidal AC voltage. The impedance of the device under test (DUT) is then represented by both its resistive (real part) and reactive (imaginary part) components. Using the equivalent capacitor model depicted in Fig. 4, the impedance can be expressed as follows:

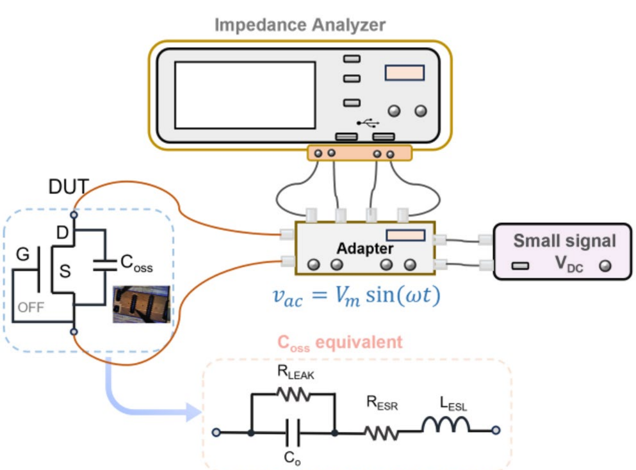

Fig. 4 Extraction of the output capacitance characteristics in GaN HEMTs

$$Z_m = R_{ESR} + \frac{R_{Leak}}{1+\omega^2 {R_{Leak}}^2 {C_o}^2} + j\frac{\omega L_{EsL} - \omega {R_{Leak}}^2 C_o + \omega^3 {R_{Leak}}^2 L_{ESL} {C_o}^2}{1+\omega^2 {R_{Leak}}^2 {C_o}^2} \tag{1}$$

An impedance analyzer or simulation can directly detect a combination of resistance and capacitance in series, represented as Cm and Rm. Consequently, the equivalent resistance and capacitance can be described as:

$$R_m = R_{ESR} + \frac{R_{Leak}}{1+\omega^2 {R_{Leak}}^2 {C_o}^2} \tag{2}$$

$$C_m = \frac{C_o + \frac{1}{\omega^2 C_o {R_{Leak}}^2}}{1 - \frac{L_{ESL}}{C_o {R_{Leak}}^2} - \omega^2 L_{ESL} C_o} \tag{3}$$

During the C_{ISS} extraction process, a constant drain-to-source voltage (V_{DS}) is maintained while the gate-to-source voltage (V_{GS}) is varied by overlaying a small sinusoidal AC signal onto a constant DC value. The total charge differential for each voltage increment is recorded, directly linked to C_{ISS}, calculated from the disparities in charge and voltage. For $\mathrm{C_{OSS}}$ extraction, with $\mathrm{V_{GS}}$ set to an appropriate level, V_{DS} is swept with an added small sinusoidal signal. The necessary charge is recorded, facilitating the calculation of C_{OSS} from the imaginary part of the impedance divided by the angular frequency (2πf). Lastly, C_{RSS} is determined by maintaining V_{DS} constant and applying a small AC signal to the gate. This process measures the drain-induced charge, correlating it to C_{RSS}. This value is derived from the variations in induced charge relative to changes in V_{GS}, assuming the transistor remains off [33].

2.4 Estimation of Proposed PV MPPT System with MATLAB Simulink

In the pursuit of realizing the proposed solar PV MPPT converter depicted in Fig. 2, MATLAB Simulink was utilized alongside the duty-cycle-controlled P&O MPPT algorithm. The objective was to configure a standalone PV system with an approximate power rating of 1 kW. To this end, a series connection of four IECS-6M6A-215 solar panels was modeled as the system's input. The simulation outputs, specifically the I-V and P-V curves for the solar array, are presented in Fig. 5 (a-b), accommodating solar irradiances ranging from 0.2 to 1 kW/m². Observations from the maximum solar irradiance reveal a PV voltage of 114.3 V at the maximum power point (MPP), while the open-circuit voltage exceeds 140 V. Conversely, the short-circuit current registers at 8 A, and the MPP current is approximately 7.5 A, aligning with the system's maximum power potential of 861.3 W.

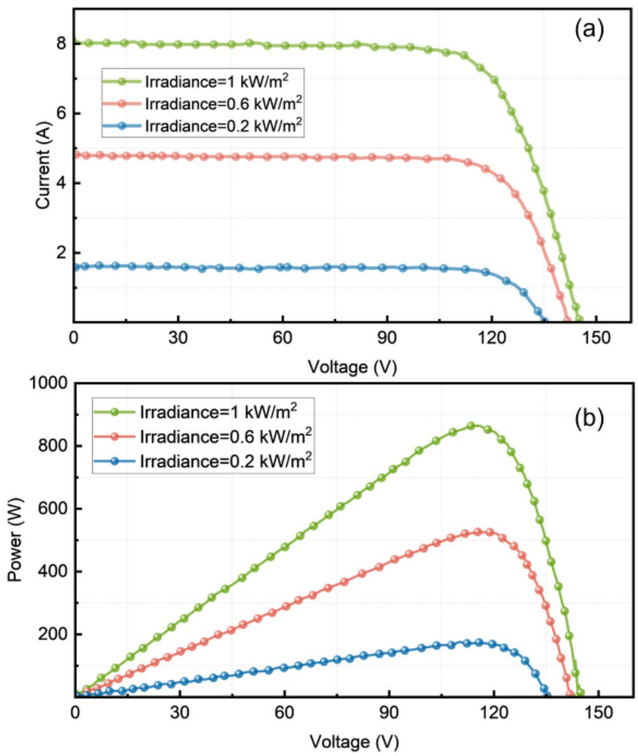

Fig. 5 MATLAB Simulink results for (**a**) I-V output curves and (**b**) P-V output curves for a 4-serious IECS-6M6A-215 solar array under irradiance of 1 kW/m^2, 0.6 kW/m^2, 0.2 kW/m^2, respectively

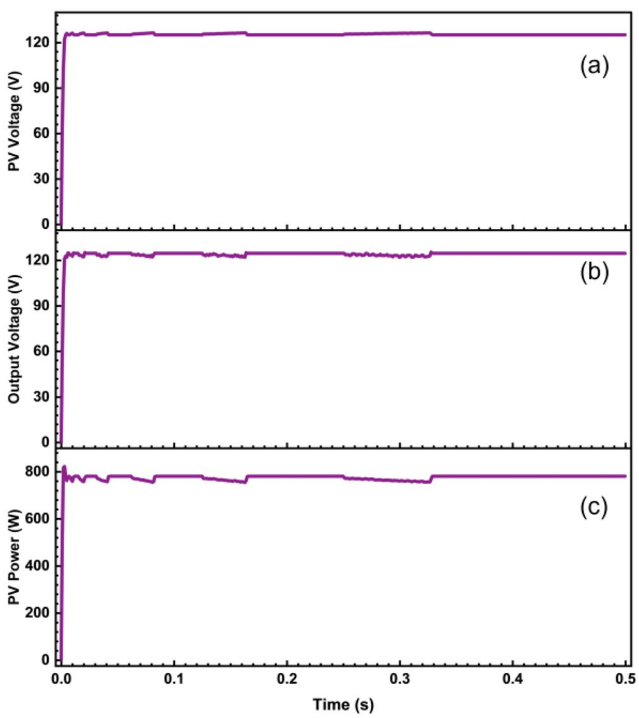

Fig. 6 MATLAB Simulink results for (**a**) PV Voltage, (**b**) Output Voltage Response, and (**c**) PV Power Response Using the Proposed Duty-Cycle-Based P&O MPPT Algorithm at a Constant Solar Irradiance of 1 kW/m²

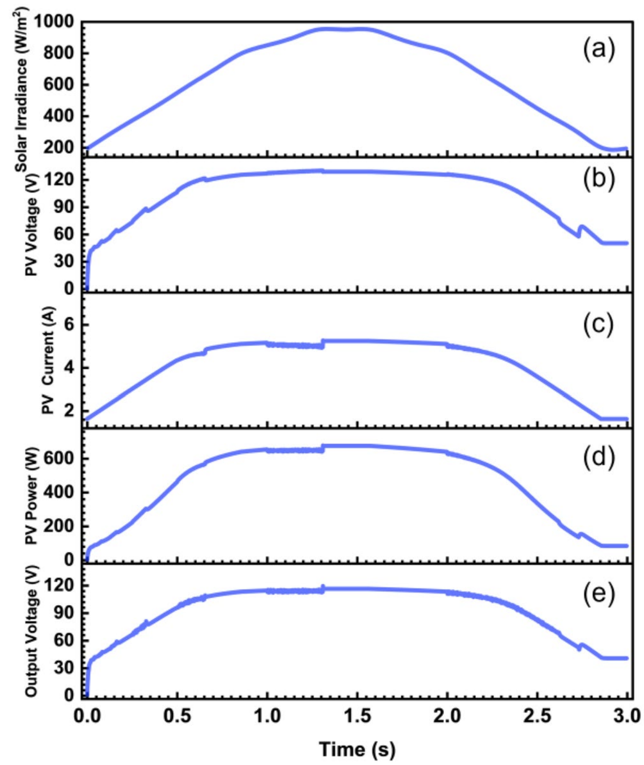

Fig. 7 MATLAB Simulink results showing: (**a**) Time-Dependent Solar Irradiance Curve, (**b**) PV Voltage Curve, (**c**) PV Current Curve, (**d**) PV Power Curve, and (**e**) Output Voltage Response Using the Proposed Duty-Cycle-Based P&O MPPT Algorithm under Time-Varying Solar Irradiance

Subsequent integration of the P&O algorithm yielded the MATLAB Simulink results showcased in Figs. 6 and 7, under variable solar irradiance scenarios. Figure 6 details the system's behavior at a steady solar irradiance of 1 kW/m², where Fig. 6(a) evidence a stabilized PV voltage to the robustness of the algorithm in a uniform irradiance environment. The output voltage response depicted in Fig. 6(b) maintains consistency, affirming the MPPT algorithm's ability to regulate voltage output effectively. Concurrently, the PV power response, as shown in Fig. 6(c), indicates a stable power output, emphasizing the duty-cycle-based P&O MPPT's role in optimizing energy capture from the solar array. In a more complex scenario with variable solar irradiance, Fig. 7(a) discloses the temporal evolution of the irradiance and the system's responsive behavior is further examined in Figs. 7(b-c), which delineate the PV voltage and current curves, demonstrating the system's resilience to environmental fluctuations. The power curve, featured in Fig. 7(d), and the output voltage response, observed in Fig. 7(e), provide insight into the system's ability to modulate its output and preserve an efficacious power yield. This informs the subsequent selection of appropriate power devices that can adequately support the observed performance spectrum, ensuring the system's overall efficacy and reliability.

3 SPICE Simulation Analysis of GaN HEMTs Under PV Converter Rating

Following the MATLAB Simulink results presented above, it is determined that for a standalone array comprising four series-connected panels, the maximum operating voltage approximates 126 V, and the load current ranges between 6 and 7 A. Within this power rating spectrum, a 200 V power device emerges as the optimal choice for the envisioned PV system design. This section delves into a comparative analysis of both static characteristics and hard switching power losses. The results encompass a SPICE simulation of a 200 V *p*-GaN HEMT against a MOSFET, each with comparable V_{DS} and I_D ratings. Additionally, a SiC FET is evaluated, noted for its higher voltage rating adhering to manufacturer standards yet maintaining a comparable terminal drain current. The selected device parameters are documented in Table 1.

3.1 Simulation Results of p-GaN HEMTs Static Transfer and Output-Capacitance Characteristics

In the preceding discussion, the significance of output capacitance within a half-bridge topology was highlighted, particularly its role in potential extra losses due to the interplay of charge cycles in adjacent switches. Moreover, transfer characteristics are deemed paramount in determining gate drive performance and informing switching circuit design. In this context, simulation results for the static transfer and output capacitance characteristics of *p*-GaN HEMTs were procured using LTSpice. Figure 8 demonstrates the transfer characteristics of GaN HEMTs relative to MOSFETs and SiC FETs, aligned with the parameters listed in their respective datasheets. The GaN HEMT is characterized by a steeper slope in the transfer characteristic curve, beginning at an approximate threshold voltage of 1.1 V, suggestive of superior transconductance. Such a feature is advantageous for high-speed switching applications, as it denotes a device that responds more promptly to variations in input voltage. Nevertheless, the possibility of inadvertent turn-on poses a risk, necessitating further optimization of dead-time control to circumvent any consequent device malfunction or failure. By contrast, the MOSFET under study is observed to commence switching at a gate voltage of 3 V, with a marginally more gradual slope in comparison. The SiC FET in question necessitates a higher gate voltage for conduction, beginning at above 4 V and exhibiting a relatively moderate slope until the V_{GS} reaches 10 V, implying the need for higher gate voltages in switching applications.

Table 1 Parameters of selected GaN HEMT, MOSFTE and SiC FET for simulation analysis

Transistor types	*p*-GaN HEMT	Si MOSFET	SiC FET
Part Numbers	EPC2215	IPP320N20N3G	E3M0060065D
V_{DS} /V	200	200	650
I_D/A	32	34	37
$V_{GS(th)}$/V	1.1	3	2.8
V_{GS}/V	-4 to +6	±20	-8 to +19
$R_{DS(on)}$/mΩ	8	32	60

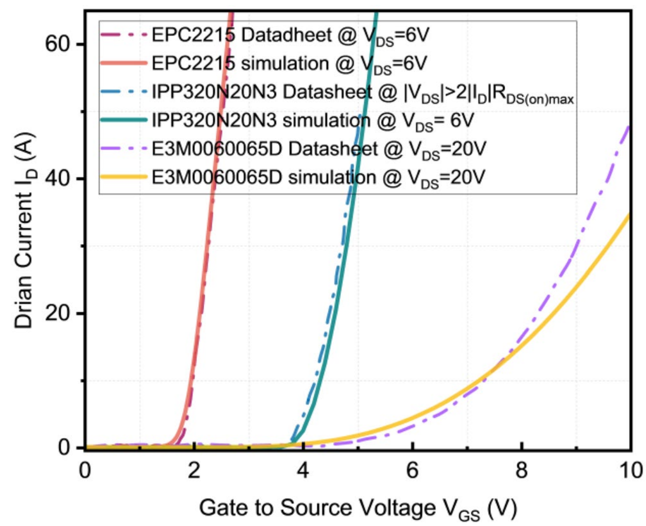

Fig. 8 Comparison of simulated and datasheet transfer characteristics for GaN HEMT, MOSFET, and SiC FET

Expanding the discussion to output capacitance—a critical factor affecting switching losses, particularly in the context of hard switching—Figure 9 presents a comparative analysis. Herewith, the GaN HEMT exhibits a reduced output capacitance in comparison to its MOSFET counterparts across a lower range of V_{DS} below 25 V. However, as the drain voltage surges past 50 V, both the MOSFET and SiC FET demonstrate lesser capacitance values in comparison to the EPC2215 GaN HEMT. Such discrepancies are attributed to the distinct LGA packaging, which accommodates multiple source and drain terminals, thereby reducing the device's footprint at the expense of heightened output stray capacitance. This increment in capacitance could entail elevated energy losses during switching, impacting the efficiency of the system. To thoroughly assess the overall power loss inherent in hard switching operations, a detailed multi-pulse test for a half-bridge setup will be elucidated.

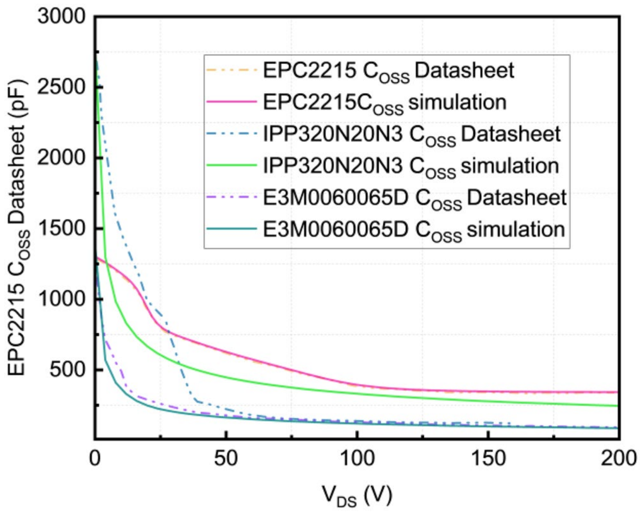

Fig. 9 Comparative analysis of simulated versus datasheet output capacitance for GaN HEMT, MOSFET, and SiC FET

3.2 Power Losses Evaluation by Multi-Pulse-Hard-Switching Half Bridge Tests

To assess the emulated switching performances of GaN HEMTs in relation to MOSFETs and SiC FETs, as well as to consider the ratings of PV MPPT output curves, a multi-pulse half-bridge hard switching simulation was performed. It is worth noting that the proposed synchronous buck converter was not utilized for the simulation due to the non-identical and unstable damping stages presented by the different switches in an open-loop buck converter configuration. Typically, such topologies employ closed-loop PI or PID control or are integrated directly with the MPPT algorithm in practical applications. To maintain consistency in the variables, an RL-loaded multi-pulse test was chosen instead, with an input voltage of 120 V. The load inductor was set to 27 µH, and the load resistor was 8 ohms. The V_{GS} for the GaN HEMT was set to 6 V, in contrast to 15 V for both the MOSFET and SiC FET. The duty cycle was configured at 0.8, with a switching frequency of 200 kHz. External parasitic inductances in the gate loop, input power loop, and common source were all accounted for, referencing our previous study, to closely replicate real switching conditions [34–36].

The result data are presented in Fig. 10. The switching waveforms for GaN HEMT, MOSFET, and SiC FET are depicted during turn-on transitions in Fig. 10(a), (c), and (e), respectively. The GaN HEMT demonstrates rapid voltage and current transitions, indicating excellent switching capability favorable for high-efficiency converter applications. However, pronounced voltage-current overlap regions observed during transitions reveal significant ringing oscillations caused by higher dv/dt and di/dt conditions, resulting in transient power losses quantified in Fig. 10(b). The MOSFET (Fig. 10(c)) shows comparatively slower switching transitions accompanied by extensive overlap regions, attributed to intrinsic parasitic capacitances and

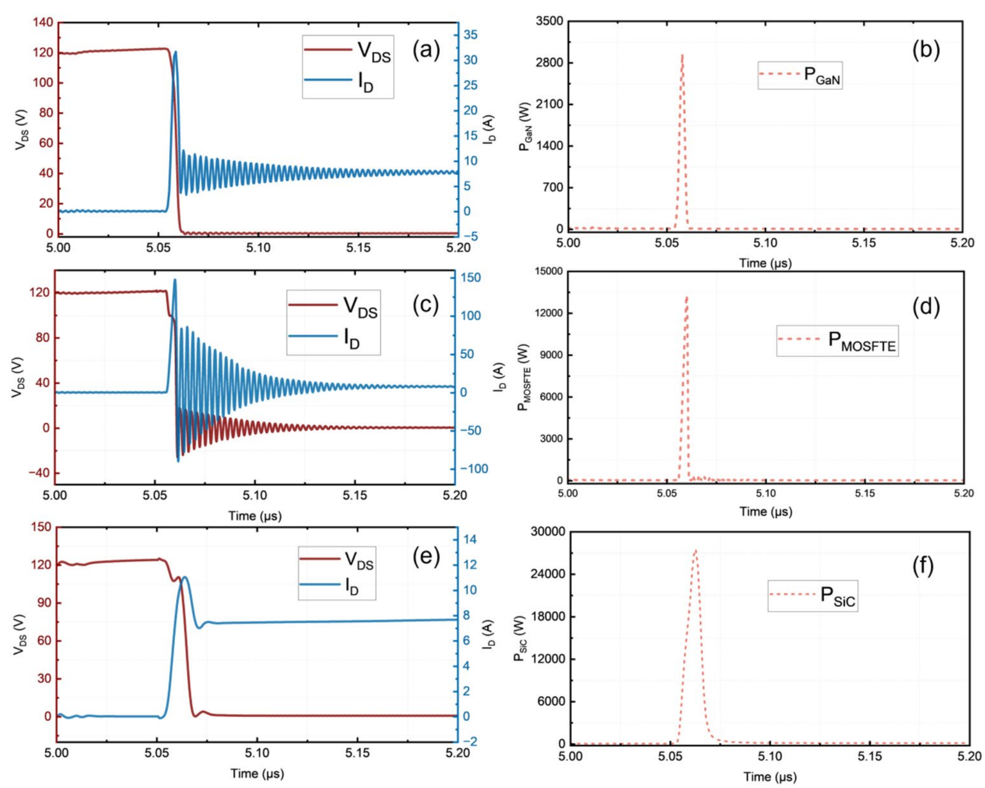

Fig. 10 SPICE-simulated-half-bridge multi-pulse hard-switching test waveforms for (**a**) GaN HEMT, (**c**) Si MOSFET, (**e**) SiC FET, Alongside Power Loss Integrals for the Switch-On Half Cycle of (**b**) GaN HEMT, (**d**) Si MOSFET, and (**f**) SiC FET

Table 2 Average power losses and energy losses in five cycles of GaN HEMT, MOSFTE and SiC FET

Transistor types	*p*-GaN HEMT	Si MOSFET	SiC FET
Average power losses (W)	4.7213	10.57	202.37
Integral of energy losses (μJ)	122.75	274.82	5261.5

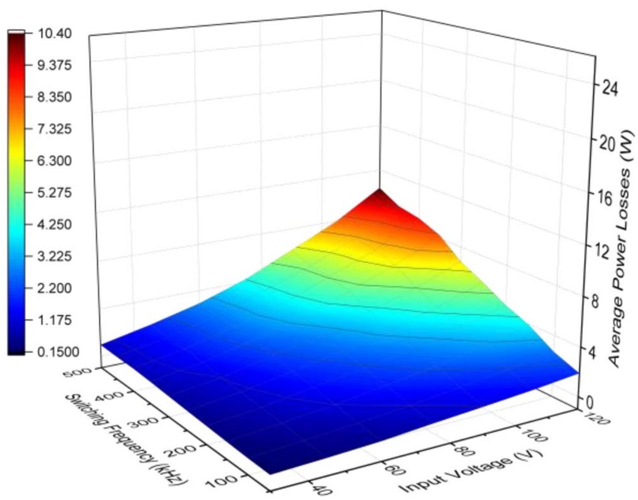

Fig. 11 3D colormap depicting average power losses of GaN HEMT in 26 μs with respect to DUT switching frequency and V_{DS}

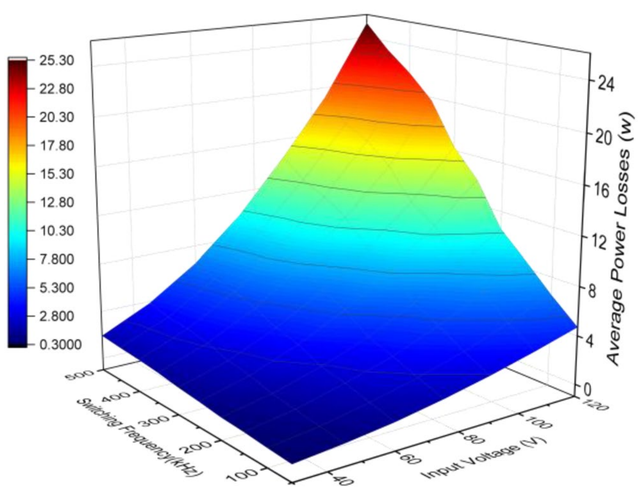

Fig. 12 3D colormap of Si MOSFET power losses over 26 μs by switching frequency and V_{DS}

inductances, indicating potential for elevated power dissipation as confirmed by the peak instantaneous power losses in Fig. 10(d). In contrast, the SiC FET depicted in Fig. 10(e) exhibits intermediate switching speed, effectively limiting the voltage-current overlap and mitigating ringing phenomena, representing a balanced performance trade-off. Nonetheless, instantaneous power losses, although reduced compared to the MOSFET, still exceed those observed in the GaN device. A detailed summary of average switching, conduction, and gate driving losses for these devices is presented in Table 2, reinforcing that GaN HEMTs exhibit superior performance for medium-voltage applications (<200 V), whereas SiC devices may serve higher-voltage, medium-frequency applications more effectively.

Based on the simulation data presented in Table 2, it is observed that at a switching frequency of 200 kHz and a V_{DS} of 120 V, the average power losses for MOSFETs are 2.4 times greater than those of GaN HEMTs. This prompts an inquiry into whether GaN HEMTs can maintain their superior switching performance over MOSFETs at lower frequencies and voltages. To address this, an expanded analysis of power losses was undertaken, the results of which are illustrated in the 3D colormaps of Figs. 11 and 12. The analysis reveals that at a reduced frequency of 50 kHz and a V_{DS} of 30 V—conditions that are theoretically advantageous for MOSFETs—the average power losses are 0.184 W for GaN HEMTs and 0.3572 W for MOSFETs, with the latter experiencing 1.94 times the initial power losses of the former. As the voltage increases to 120 V under the same low frequency, the disparity in power loss widens, with MOSFETs incurring 2.47 times the losses of GaN HEMTs. Conversely, at a high frequency of 500 kHz and a V_{DS} of 30 V, the initial power loss ratio for MOSFETs rises to 2.0 compared to 1.94 at 50 kHz. As the voltage escalates to 120 V, this ratio further increases to 2.43. This quantitative comparison underscores the superior performance of GaN HEMTs, especially at elevated voltages and frequencies. In conclusion, the colormaps in Figs. 11 and 12 support a detailed comparative assessment of the two device technologies. The results confirm that GaN HEMTs exhibit favorable characteristics across all operational regimes. The 2DEG configuration in GaN HEMTs facilitates enhanced electron mobility and accelerated switching rates relative to traditional P-N junctions in MOSFETs. This leads to less overlap between voltage and current during switching transitions, thereby reducing switching losses. The improved efficiency of GaN HEMTs not only confirms the theoretical benefits but also has considerable ramifications for the overall performance of PV systems. In practical situations, particularly in distant applications where maintenance is difficult, enhanced efficiency and less heat stress led to increased dependability and durability of photovoltaic systems. Thus, GaN HEMT-based converters provide an optimal selection for stand-alone PV MPPT converters, improving energy extraction and system reliability.

4 Conclusion

This work illustrates the effectiveness of a simulation-based method that combines MATLAB Simulink and SPICE simulation to evaluate 200 V Schottky *p*-GaN HEMTs in photovoltaic MPPT buck converters, emphasizing the enhanced efficiency of GaN devices compared to conventional MOSFETs in renewable energy applications. The study highlights the significant impact of C_{OSS} extraction, demonstrating GaN's remarkable ability to decrease average power losses during hard-switching cycles by a factor of 2.24 relative to MOSFETs. This was accomplished by a meticulous evaluation of a duty cycle-controlled P&O MPPT algorithm and an extensive examination under fluctuating irradiance conditions. Although the results are encouraging, they rely on simulations, and real-world application may pose more difficulties. The research focuses on certain operating circumstances and device characteristics, which may differ across various applications. Future research should include experimental confirmation of the simulation results, examination of GaN HEMTs in other converter topologies, assessment of long-term dependability under diverse environmental circumstances, and refinement of control algorithms for improved performance. These initiatives will further validate the capability of GaN HEMTs in enhancing PV MPPT buck converters and expedite the shift towards dependable and efficient worldwide renewable energy options. Moreover, exploring practical implementations in large-scale and grid-connected PV systems could significantly advance the adoption of GaN HEMTs in renewable energy infrastructures.

Supplementary Information The online version contains supplementary material available at https://doi.org/10.1007/s42835-025-02334-y.

Acknowledgements The authors express their profound gratitude to Universiti Putra Malaysia for the vital support received through the Geran Putra (GP)-IPM/2022/9732100 grant. This financial backing has been instrumental in advancing and facilitating our research endeavors.

Author Contributions Xinzhi Liu: Conceptualization, Methodology, Software, Investigation, Formal analysis, Data curation, Writing – Original Draft, Writing – review & editing, Visualization, Project administration. Suhaidi Shafie: Conceptualization, Methodology, Resources, Visualization, Writing – review & editing, Supervision, Project administration, Funding acquisition. Mohd Amran Mohd Radiz: Conceptualization, Methodology, Writing – review & editing, Supervision. Norhafiz Azis: Supervision, Project administration, Funding acquisition. Abdul Hafiz Abdul Karim: Resources, Writing – review & editing. Nurbahirah Norddin: Resources, Writing – review & editing. Ismail Lawal: Resources, Writing – review & editing.

Funding Open access funding provided by The Ministry of Higher Education Malaysia and Universiti Putra Malaysia

Data Availability The data supporting the findings of this study are available from the corresponding author upon reasonable request.

Declarations

Conflicts of Interest The authors declare that there are no conflicts of interest regarding the publication of this paper. This statement confirms that the authors have no financial, personal, or professional affiliations that could be perceived as influencing the research or its interpretation.

References

1. Brockway PE, Owen A, Brand-Correa LI, Hardt L (Jul. 2019) Estimation of global final-stage energy-return-on-investment for fossil fuels with comparison to renewable energy sources. Nat Energy 4(7):612–621. https://doi.org/10.1038/s41560-019-0425-z
2. Ahmad S, Kadir MZAA, Shafie S (Feb. 2011) Current perspective of the renewable energy development in Malaysia. Renew Sustain Energy Rev 15(2):897–904. https://doi.org/10.1016/j.rser.2010.11.009
3. Shokouhandeh H, Ahmadi Kamarposhti M, Asghari F, Colak I, Eguchi K (Apr. 2022) Distributed generation management in smart grid with the participation of electric vehicles with respect to the vehicle owners' opinion by using the imperialist competitive algorithm. Sustainability 14(8):4770. https://doi.org/10.3390/su14084770
4. Shokouhandeh H, Ahmadi Kamarposhti M, Colak I, Eguchi K (Sep. 2021) Unit commitment for power generation systems based on prices in smart grid environment considering uncertainty. Sustainability 13(18):10219. https://doi.org/10.3390/su131810219
5. Liu X, Shafie S (Aug. 2024) Nanostructure silver absorbance with polarized light spectroscopy (PLS) and mobile imaging. Instrum Sci Technol 1–14. https://doi.org/10.1080/10739149.2024.2396138
6. Wang R, Liu X, Shafie S (Jun. 2024) Evaluating perovskite solar panels for thermal stability and inclination performance through finite element modelling. Eng Res Express 6(2):025327. https://doi.org/10.1088/2631-8695/ad43bb
7. Eslami E, Ahmadi Kamarposhti M (Dec. 2019) Optimal design of solar–wind hybrid system-connected to the network with cost-saving approach and improved network reliability index. SN Appl Sci 1(12):1742. https://doi.org/10.1007/s42452-019-1710-y
8. Makahleh FM et al (2023) Optimal management of energy storage systems for peak shaving in a smart grid. Computers Mater Continua 75(2):3317–3337. https://doi.org/10.32604/cmc.2023.035690
9. Kamarposhti MA, Colak I, Shokouhandeh H, Iwendi C, Padmanaban S, Band SS (Jan. 2025) Optimum operation management

of microgrids with cost and environment pollution reduction approach considering uncertainty using multi-objective NSGAII algorithm. IET Renew Power Gener 19(1). https://doi.org/10.1049/rpg2.12579
10. Lawal et al (Mar. 2025) Maximizing solar energy harvesting: enhancing the efficiency of bifacial dye-sensitized solar cells with graphenated carbon nanotubes composites in multi-layered stacked photoanode. Opt Mater (Amst) 160:116721. https://doi.org/10.1016/j.optmat.2025.116721
11. Duffie JA (Deceased), Beckman WA, Blair N (eds) (2020) Solar engineering of thermal processes, photovoltaics and wind. Wiley. https://doi.org/10.1002/9781119540328
12. Tiedje T, Yablonovitch E, Cody GD, Brooks BG (May 1984) Limiting efficiency of silicon solar cells. IEEE Trans Electron Devices 31(5):711–716. https://doi.org/10.1109/T-ED.1984.21594
13. Li J, Yu T (Sep. 2021) Distributed deep reinforcement learning for optimal voltage control of PEMFC. IET Renewable Power Generation 15(12):2778–2798. https://doi.org/10.1049/rpg2.12202
14. Aghabalaei V, Nayeb H, Mardani S, Tabeshnia M, Baghdadi M (Dec. 2023) Minimizing greenhouse gases emissions and energy consumption from wastewater treatment plants via rational design and engineering strategies: a case study in Mashhad, Iran. Energy Reports 9:2310–2320. https://doi.org/10.1016/j.egyr.2023.01.017
15. Kim S, Jahandar M, Jeong JH, Lim DC (Nov. 2019) Recent progress in solar cell technology for low-light indoor applications. Curr Altern Energy 3(1):3–17. https://doi.org/10.2174/1570180816666190112141857
16. Aryanezhad M (Apr. 2017) Fuzzy-decision-making predictive power control approach to on-grid photovoltaic panel. In: Conference on Electrical Power Distribution Networks Conference (EPDC). IEEE, pp 137–142. https://doi.org/10.1109/EPDC.2017.8012754
17. Aryanezhad M (Mar. 2022) A robust game-theoretic optimization model for battery energy storage in multi-microgrids by considering of renewable based DGs uncertainty. Electr Power Syst Res 204:107591. https://doi.org/10.1016/j.epsr.2021.107591
18. Aryanezhad M (Sep. 2018) Management and coordination of LTC, SVR, shunt capacitor and energy storage with high PV penetration in power distribution system for voltage regulation and power loss minimization. Int J Electr Power Energy Syst 100:178–192. https://doi.org/10.1016/j.ijepes.2018.02.015
19. Roccaforte F et al (Feb. 2018) Emerging trends in wide band gap semiconductors (SiC and GaN) technology for power devices. Microelectron Eng 187–188. https://doi.org/10.1016/j.mee.2017.11.021
20. Chen KJ et al (Mar. 2017) GaN-on-Si power technology: devices and applications. IEEE Trans Electron Devices 64(3):779–795. https://doi.org/10.1109/TED.2017.2657579
21. Jones EA, Wang FF, Costinett D (Sep. 2016) Review of commercial GaN power devices and GaN-based converter design challenges. IEEE J Emerg Sel Top Power Electron 4(3):707–719. https://doi.org/10.1109/JESTPE.2016.2582685
22. Nakajima Y, Sumida MH, Dhyani H, Kawai EMS, Narayanan (Dec. 2010) High density two-dimensional hole gas induced by negative polarization at GaN/AlGaN heterointerface. Appl Phys Express 3(12):121004. https://doi.org/10.1143/APEX.3.121004
23. Zhong Y et al A review on the GaN-on-Si power electronic devices. May 01 2022 KeAi Commun Co https://doi.org/10.1016/j.fmre.2021.11.028
24. Hou R, Shen Y, Zhao H, Hu H, Lu J, Long T (Jun. 2020) Power loss characterization and modeling for GaN-based hard-switching half-bridges considering dynamic on-state resistance. IEEE Trans Transp Electrification 6(2):540–553. https://doi.org/10.1109/TTE.2020.2989036
25. Akira Nakajima K, Takao M, Shimizu H, Okumura H, Ohashi (Sep. 2008) Equivalent circuit model for GaN-HEMTs in a switching simulation. In: INTELEC 2008–2008 IEEE 30th International telecommunications energy conference. IEEE, pp 1–4. https://doi.org/10.1109/INTLEC.2008.4664095
26. Liu X et al (Apr. 2024) SPICE modeling and performance analysis of enhancement-mode GaN HEMTs for augmented hard-switching energy conversion efficiency. Pertanika J Sci Technol 32(3):1243–1262. https://doi.org/10.47836/pjst.32.3.14
27. Suskis P (Nov. 2014) Simulation of synchronous boost MPPT converter with GaN switches for photovoltaics. In: IEEE 2nd Workshop on Advances in Information, Electronic and Electrical Engineering (AIEEE). IEEE, pp 1–4. https://doi.org/10.1109/AIEEE.2014.7020322
28. Alharbi SS, Matin M (Sep. 2021) Experimental evaluation of medium-voltage cascode gallium nitride (GaN) devices for bidirectional DC-DC converters. CES Transactions on Electrical Machines and Systems 5(3):232–248. https://doi.org/10.30941/CESTEMS.2021.000227
29. Koszel M, Grzejszczak P, Nowatkiewicz B, Wolski K (Dec. 2020) Design, analysis and comparison of Si- and GaN-based DC-DC wide-input-voltage-rangeBuck-boost converters. Int J Electron Telecommun 337–343. https://doi.org/10.24425/ijet.2021.135986
30. Mdanat RAL, Georgious R, Garcia J, De Donato G, Capponi FG (Nov. 2020) Characterization of GaN HEMT transistors for DC/DC converters in transportation applications. In: 2020 IEEE Vehicle Power and Propulsion Conference (VPPC). IEEE, pp 1–6. https://doi.org/10.1109/VPPC49601.2020.9330991
31. Alharbi SS, Alharbi SS, Al-bayati AMS, Matin M (Nov. 2017) A highly efficient non-isolated DC-DC buck-boost converter with a cascode GaN-FET and SiC-Schottky diode. In: IEEE Conference on Technologies for Sustainability (SusTech). IEEE, pp 1–6. https://doi.org/10.1109/SusTech.2017.8333529
32. Perera N, Jafari A, Soleimanzadeh R, Bollier N, Abeyratne SG, Matioli E (Jul. 2022) Hard-switching losses in power FETs: the role of output capacitance. IEEE Trans Power Electron 37(7):7604–7616. https://doi.org/10.1109/TPEL.2021.3130831
33. Matioli E, Zhu H, Perera N, Nikoo MS, Jafari A, van Erp R (Sep. 2023) Switching losses in power devices: from dynamic on resistance to output capacitance hysteresis. In: 2023 25th European Conference on Power Electronics and Applications (EPE'23 ECCE Europe). IEEE, pp 1–7. https://doi.org/10.23919/EPE23ECCEEurope58414.2023.10264510
34. Liu X, Shafie S, Radzi MAM, Azis N, Karim AHA (Jan. 2024) Modelling and mitigating Oscillation in E-mode GaN HEMT: A simulation-based approach to parasitic inductance optimization. Microelectron Reliab 152:115293. https://doi.org/10.1016/j.microrel.2023.115293
35. Liu X, Shafie S, Amran Mohd M, Radzi N, Azis (Sep. 2024) SPICE simulation Assisted-Dynamic Rds(on) characterization in 200V commercial Schottky p-GaN HEMTs under unstable phases. J Phys Conf Ser 2841(1):012001. https://doi.org/10.1088/1742-6596/2841/1/012001
36. Liu X, Hua M, Shafie S, Radzi MAM, Azis N (Aug. 2024) SPICE Modelling-Assisted evaluation of dynamic on-resistance characterization in Schottky p-GaN HEMTs amid synchronous Buck transient instabilities. Comput Electr Eng 118:109410. https://doi.org/10.1016/j.compeleceng.2024.109410

Xinzhi Liu is a Ph.D. candidate at Universiti Putra Malaysia, Selangor, Malaysia. He received an Honors Diploma in Electrical Engineering Technology from Red River Polytechnic, Manitoba, Canada, in 2020. In 2022, he earned his M.Sc. degree in Physics from Hong Kong Baptist University, HKSAR. He is a visiting Ph.D. for the 2023–2025 period at the Southern University of Science and Technology (SUSTech), Shenzhen, China. His research interests include circuit design, power electronics, SPICE simulations, GaN HEMT, SiC MOSFET, DC-DC converters, solar PV energy, and perovskite solar cells.

Suhaidi Shafie is a highly experienced academic and accomplished researcher with an extensive background in electrical and electronics engineering. He obtained his Bachelor of Engineering in Electrical and Electronics from the University of the Ryukyus, Japan in 2000, and worked as a Design Engineer at ALPS Electric (M) Sdn. Bhd. from 2000 to 2002. Dr. Suhaidi completed his Master of Engineering and Doctor of Engineering degrees in Electrical and Electronics, specializing in Nanovision, from Tokyo University of Agriculture and Technology and Shizuoka University, respectively, in 2005 and 2008. Currently, he is a Full Professor at Universiti Putra Malaysia. Dr. Suhaidi's research focuses on optical devices, circuits, and systems, including Solar Cell, Solar Photovoltaic, Sensors, and Analog IC interfacing circuits. He previously served as the Head of the Functional Devices Laboratory at the Institute of Advanced Technology, Universiti Putra Malaysia, from 2015 to 2021. Dr. Shafie was also the chapter chair of the IEEE Circuits and Systems Society Malaysia Chapter for 2017 and 2018. He is certified as a Professional Engineer and Professional Technologies by the Board of Engineer Malaysia and the Malaysian Board of Technologist, respectively.

Mohd Amran Mohd Radzi received a PhD degree in 2010 from the University of Malaya. He is Professor in Power and Energy at Department of Electrical and Electronic Engineering, Faculty of Engineering, Universiti Putra Malaysia (UPM). He is also Researcher for Advanced Lightning, Power, and Energy Research (ALPER) Centre, UPM. His main areas of expertise are power electronics, power quality, and renewable energy. Prof. Dr. Mohd Amran is Chartered Engineer, U.K., and Senior Member of IEEE.

Norhafiz Azis received the B.Eng. degree in electrical and electronic engineering from Universiti Putra Malaysia, in 2007, and the Ph.D. degree in electrical and electronic engineering from The University of Manchester, U.K., with a focus on the power transformer. Currently, he is an Associate Professor with the Faculty of Engineering, Universiti Putra Malaysia. He is the Head of the Advanced Lightning, Power and Energy Research Centre (ALPER). His research interests include in-service aging of transformer insulation, condition monitoring, asset management, and alternative insulation materials for transformers.

Abdul Hafiz Abdul Karim graduated with a Bachelor of Engineering (Electrical Electronic Engineering) and Master of Engineering (Electrical Electronic System Engineering) from Tokai University. He is currently pursuing a PhD degree in Power Engineering in Universiti Putra Malaysia (UPM). He is a registered Graduate Engineer under the Board of Engineers Malaysia (BEM). His research interests are Power Engineering, Energy Storage and Electric Vehicles.

Nurbahirah Norddin received her B. Eng Degree in Electrical Engineering (Power Electronics and Drives) in 2011 and M. Eng in Electrical Engineering from Universiti Teknikal Malaysia Melaka (UTeM) in 2014. She is a lecturer in Universiti Teknikal Malaysia Melaka (UTeM). Currently, she is pursuing her Doctor of Philosophy in Universiti Putra Malaysia (UPM) in solar cell research. Her interest involves high voltage, signal processing and perovskite solar cell.

Ismail Lawal is a graduate of electrical engineering (B. Eng) and holds a master's Degree in Control and Instrumentation Engineering (M. Eng) all the from Bayero university Kano, Nigeria. he is currently pursuing PhD at the department of electrical and electronics Engineering in the University Putra Malaysia (UPM) with research interest in renewable energy and focus on Solar cells. He works with the Nigeria's National Agency for science and engineering infrastructure as a principal research officer.